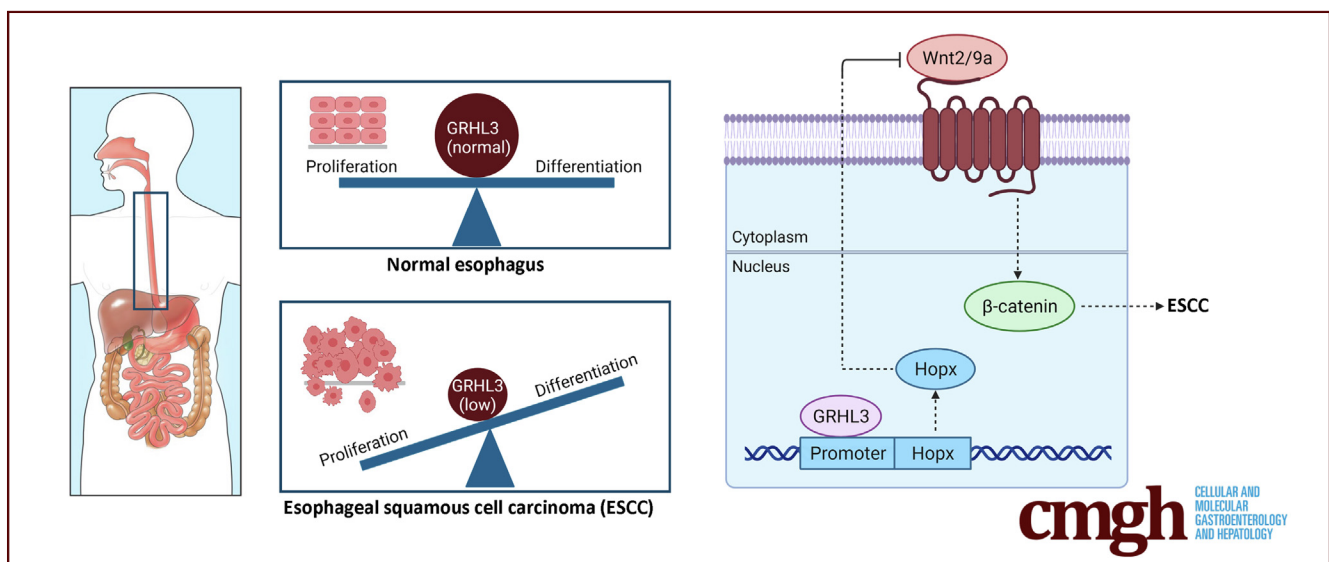


ORIGINAL RESEARCH

Identification of a Novel GRHL3/HOPX/Wnt/ β -Catenin Proto-oncogenic Axis in Squamous Cell Carcinoma of the Esophagus

Smitha Rose Georgy,¹ Diar Riyanti Rudiantmoko,² Alana Auden,³ Darren Partridge,³ Tariq Butt,³ Seema Srivastava,³ Nick Wong,⁴ Dijina Swaroop,³ Marina Rose Carpinelli,³ Mirjana Bogeski,¹ and Stephen M. Jane³

¹Department of Anatomic Pathology, Faculty of Veterinary and Agricultural Sciences, The University of Melbourne, Werribee, Australia; ²Department of Otorhinolaryngology, Faculty of Medicine, Universitas Indonesia, Indonesia; ³Department of Medicine, Central Clinical School, Monash University, Melbourne, Australia; and ⁴Monash Bioinformatics Platform, Central Clinical School, Melbourne, Australia



SUMMARY

The transcription factor GRHL3 exerts its tumor suppressor function in esophageal squamous cell carcinoma through regulating HOPX expression and Wnt signaling. The study provides a clear rationale for using targeted therapies against Wnt/ β -catenin pathways in patients with reduced GRHL3 expression.

BACKGROUND & AIMS: Esophageal squamous cell carcinoma (ESCC) is an aggressive malignancy with a poor long-term prognosis. The molecular mechanisms underlying the initiation and progression of this tumor are largely unknown. The transcription factor GRHL3 functions as a potent tumor suppressor in SCC of skin, head, and neck. This study aims to determine whether GRHL3 also plays a role in the homeostasis of the esophageal epithelium and in the development of ESCC.

METHODS: The effects of *Grhl3* deletion on squamous epithelial homeostasis in embryos and adult mice were examined using immunohistochemistry, transmission electron microscopy, and real-time polymerase chain reaction. The conditionally deleted mice were subsequently used to determine

susceptibility to ESCC. Whole-transcriptome sequencing (RNA-seq) was performed on ESCC in wild-type and *Grhl3* deleted animals. To decipher the signaling pathways, real-time polymerase chain reaction, immunohistochemistry, analysis of chromatin immunoprecipitation sequencing, chromatin immunoprecipitation-polymerase chain reaction, and RNA seq datasets were used. Primary human samples were used to validate the findings in the mouse model.

RESULTS: Loss of *Grhl3* perturbs the proliferation-differentiation balance in the esophageal epithelium, thereby increasing the susceptibility to esophageal carcinogenesis in adult mice. *Grhl3* imparts its tumor suppressor function by regulating the expression of HOPX. We have identified the Wnt/ β -catenin pathway as the downstream effectors of GRHL3 and HOPX through our integrated approach using patient-derived ESCC samples and mouse models.

CONCLUSIONS: GRHL3 conveys its tumor suppressor function in ESCC through regulating its target gene HOPX, which limits Wnt/ β -catenin signaling. Targeted therapies to inhibit this pathway could be a potential treatment strategy for ESCC patients with reduced GRHL3 expression. (*Cell Mol Gastroenterol Hepatol* 2023;15:1051–1069; <https://doi.org/10.1016/j.jcmgh.2022.11.009>)

Keywords: Transcriptional Regulation; Cancer Signaling Pathways; RNA Sequencing.

Esophageal squamous cell carcinoma (ESCC) accounts for 90% of all cases of esophageal malignancies globally. It is one of the most common and aggressive malignancies, with high prevalence in Eastern Asia, Southern and Eastern Africa, and Northern and Western Europe.¹ Most patients present with locally advanced cancer requiring extensive treatment, including chemotherapy, chemoradiotherapy, and/or surgical resection.² Even though there has been a marginal reduction in the incidence of ESCC, the medial survival of ESCC has remained unchanged at 5–13 months since the 1990s.³ The poor long-term prognosis relates to a lack of treatment options resulting from a dearth of understanding into the molecular mechanisms that underlie the initiation and progression of the tumor. Hence it is vital to identify the molecular pathogenesis of ESCC and to develop novel therapeutic targets.

Genes dysregulated in ESCC include those involved in cell cycle regulation, receptor tyrosine kinases, chromatin remodeling factors, and genes that perturb squamous cell proliferation/differentiation balance.² The proliferating cells of the esophagus are confined to the basal cell layer, and imbalance of proliferation/differentiation induces the emergence of preneoplastic epithelium.⁴ One gene that maintains this balance in a variety of tissues encodes the transcription factor Grainyhead like 3 (GRHL3), shown in *in vivo* models to be essential for epidermal development and skin barrier formation.^{5,6} *Grhl3* also exhibits critical suppressor function in both skin and oral epithelium, and its loss induces SCC at both sites,^{7,8} particularly with carcinogen exposure. In the skin, this is mediated by a Grhl3/PTEN/AKT proto-oncogenic axis,⁷ whereas in head and neck SCC, oncogenesis is driven by dysregulated GSK3B/C-Myc expression.⁸ Identification of these tissue-specific transcriptional target genes that drive malignancy in the skin and oral epithelium prompted us to investigate the consequences of loss of GRHL3 in the esophageal epithelium.

Results

Grhl3 Deletion During Embryogenesis Causes Hyperproliferation of the Esophageal Epithelium

The mouse embryonic esophagus is initially lined by columnar epithelium, which converts to squamous epithelium between embryonic day (E) 10.5 and 14.5.⁹ During this conversion, the epithelial cells exhibit a reduction in keratin (K) 8 expression and gain in K14 expression. Previous studies in wild-type (WT) mice demonstrated expression of *Grhl3* in the developing esophagus from E10.5, which persisted throughout development.¹⁰ To examine the effects of loss of *Grhl3* on esophageal development, we initially focused on the constitutive *Grhl3*-null mice, which carry *LacZ* genes that report from the null alleles.¹¹ Because these animals die at birth of skin barrier and neural tube defects, we harvested mice at E18.5 for analysis. Immunohistochemistry (IHC) detecting β -galactosidase revealed high level expression in esophageal epithelium of *Grhl3*^{-/-} mice


(Figure 1A), with similar staining patterns in the proximal and distal esophagus (not shown). Staining was even throughout the suprabasal layers, with almost complete sparing of the basal layer reminiscent of *Grhl3* staining in the developing epidermis.¹² The presence of Grhl3 protein expression in WT and its absence in KO embryonic esophagus were confirmed using IHC (Figure 1B). Histologically, the esophageal epithelium of *Grhl3*^{-/-} mice was thicker compared with *Grhl3*^{+/+} mice (Figure 1C and D), with more nucleated cells in the spinous and granular layers (Figure 1E), similar to the appearance of the *Grhl3*-null epidermis.¹² These changes were accompanied by a marked increase in the number of proliferating cells as assessed by Ki67 IHC (Figure 1F and G). No difference in the number of caspase 3-positive apoptotic cells was observed (Figure 1H).

To assess the effects of loss of *Grhl3* on the balance between proliferation and differentiation, we examined the expression of a variety of keratin genes. K6, a marker of hyperproliferation that is elevated in the context of epithelial damage, was markedly increased in the esophageal epithelium of *Grhl3*^{-/-} mice compared with WT embryos (Figure 2A), mimicking the up-regulation we see in the *Grhl3*-null epidermis. Expression of K8 was also aberrant in the *Grhl3*-null esophagus, detectable in both basal and suprabasal layers, unlike the WT esophageal epithelium where it was mainly confined to suprabasal layers and markedly reduced expression in the cell membrane of the basal layers (Figure 2B). K5 and K14, which normally mark proliferating cells in the basal layer, and K4, a marker of differentiated suprabasal cells, remained largely unchanged, although K13, another suprabasal marker, was marginally enhanced (Figure 2C–F). Taken together, these results are indicative of a perturbation in the proliferation-differentiation equilibrium of the esophageal epithelium in the absence of *Grhl3*.

Grhl3 Deletion Is a Driver of Esophageal Squamous Cell Carcinoma

To examine *Grhl3* expression in the adult esophagus, we analyzed sections from the *Grhl3*^{+/-} mice with X-gal staining and β -galactosidase IHC. Robust expression was present in the suprabasal layers of the squamous epithelium, again with almost complete absence in the basal layer (Figure 3). To allow investigation of the functional role of *Grhl3* in the adult esophagus, we generated a *Grhl3* conditional knockout (*Grhl3*cKO) line using an EBV ED-L2Cre transgene. The EBV ED-L2 promoter targets expression specifically to the tongue, esophagus, and forestomach but not the skin,

Abbreviations used in this paper: 4NQO, 4-nitroquinolene-1 oxide; ChIP, chromatin immunoprecipitation; ESCC, esophageal squamous cell carcinoma; GRHL3, Grainyhead like 3; *Grhl3*-cKO, *Grhl3*-conditional knockout; IHC, immunohistochemistry; K, keratin; Q-RT-PCR, quantitative real-time polymerase chain reaction; WT, wild-type.

 Most current article

© 2022 The Authors. Published by Elsevier Inc. on behalf of the AGA Institute. This is an open access article under the CC BY-NC-ND license (<http://creativecommons.org/licenses/by-nc-nd/4.0/>).

2352-345X

<https://doi.org/10.1016/j.jcmgh.2022.11.009>

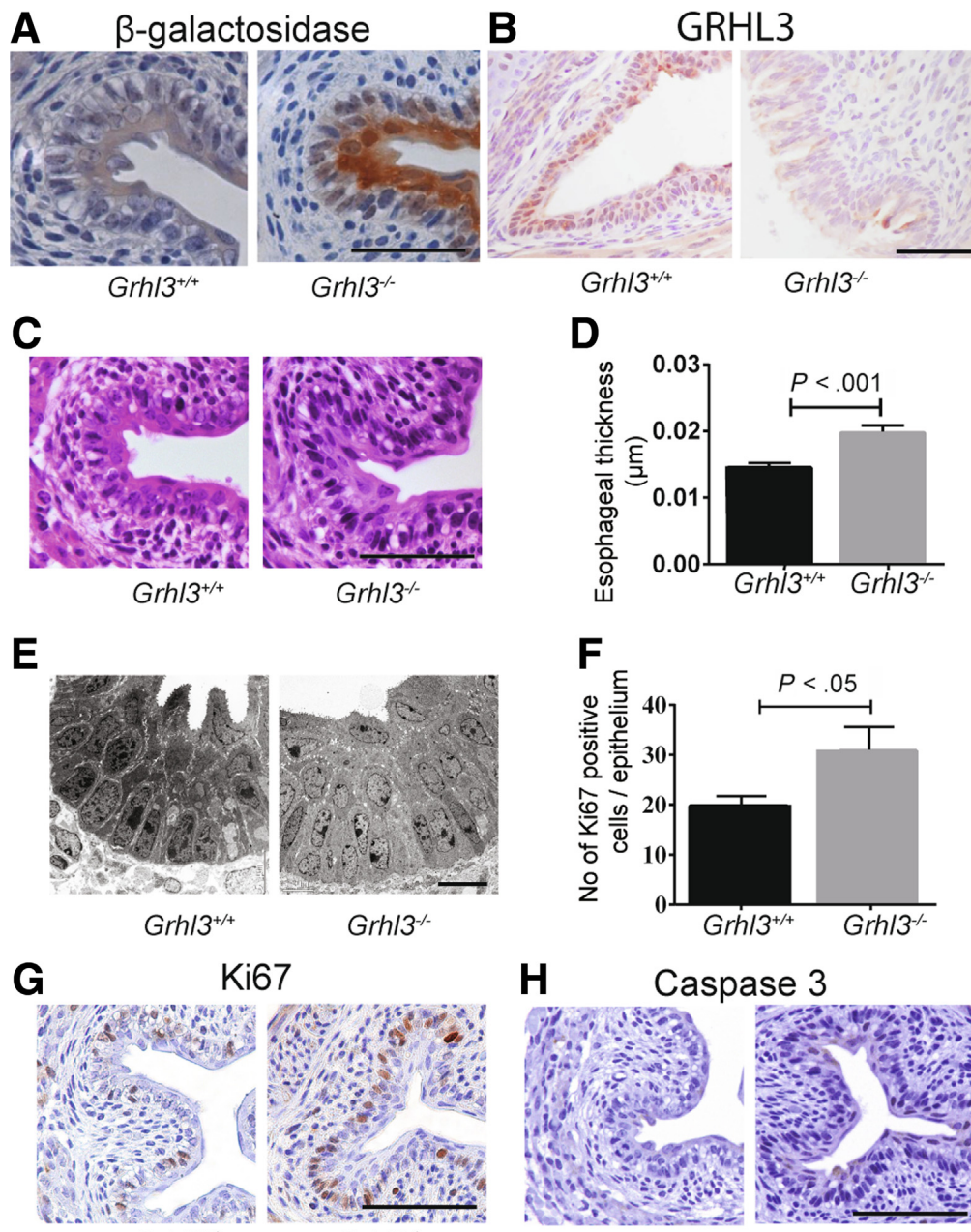


Figure 1. *Grhl3* deletion during embryogenesis causes hyperproliferation of the esophageal epithelium. (A and B) Representative images of transverse sections of the middle esophagus of E18.5 wild-type (*Grhl3*^{+/+}) and *Grhl3*-knockout (*Grhl3*^{-/-}) mice ($n = 3$ each) immunohistochemically analyzed with β -galactosidase and Grhl3. Scale bar = 50 μm . (C) Representative H&E images of *Grhl3*^{+/+} and *Grhl3*^{-/-} mice middle esophagus showing increased thickness of esophageal epithelium in *Grhl3*^{-/-} mice. Scale bar = 50 μm . (D) Esophageal epithelial thickness was quantified from H&E images of E18.5 *Grhl3*^{+/+} and *Grhl3*^{-/-} mice ($n = 3$ each) using ImageJ software. Three sections representing cervical, thoracic, and abdominal areas were examined, and 4 points per section were measured to calculate the average thickness of the esophagus. Statistics were calculated using unpaired, two-tailed Student t test. (E) Representative transmission electron micrograph of E18.5 *Grhl3*^{+/+} and *Grhl3*^{-/-} mice middle esophagus ($n = 3$ each). Nucleated suprabasal squamous epithelium shown in *Grhl3*^{-/-} embryo esophagus. Scale bar = 50 μm . (F) Graph shows number of Ki67 positive cells in the esophagus in E18.5 *Grhl3*^{+/+} and *Grhl3*^{-/-} mice ($n = 3$ each), enumerated from micrographs immunohistochemically analyzed with Ki67 (representative image shown, G). Statistics were calculated using unpaired, two-tailed Student t test ($*P < .05$). (H) Representative immunohistochemical images of E18.5 *Grhl3*^{+/+} and *Grhl3*^{-/-} mice middle esophagus ($n = 3$ each) stained with caspase antibody. Scale bar = 50 μm .

avoiding both neural tube and skin barrier defects that are lethal for the constitutive knockouts.¹³ Mice were engineered to carry a constitutively deleted allele (*Grhl3*⁻) and

an undeleted floxed allele (*Grhl3*^{fl}) that could be deleted with exposure to the *Cre* recombinase to generate the conditional null allele (*Grhl3* ^{Δ}). We have used this strategy

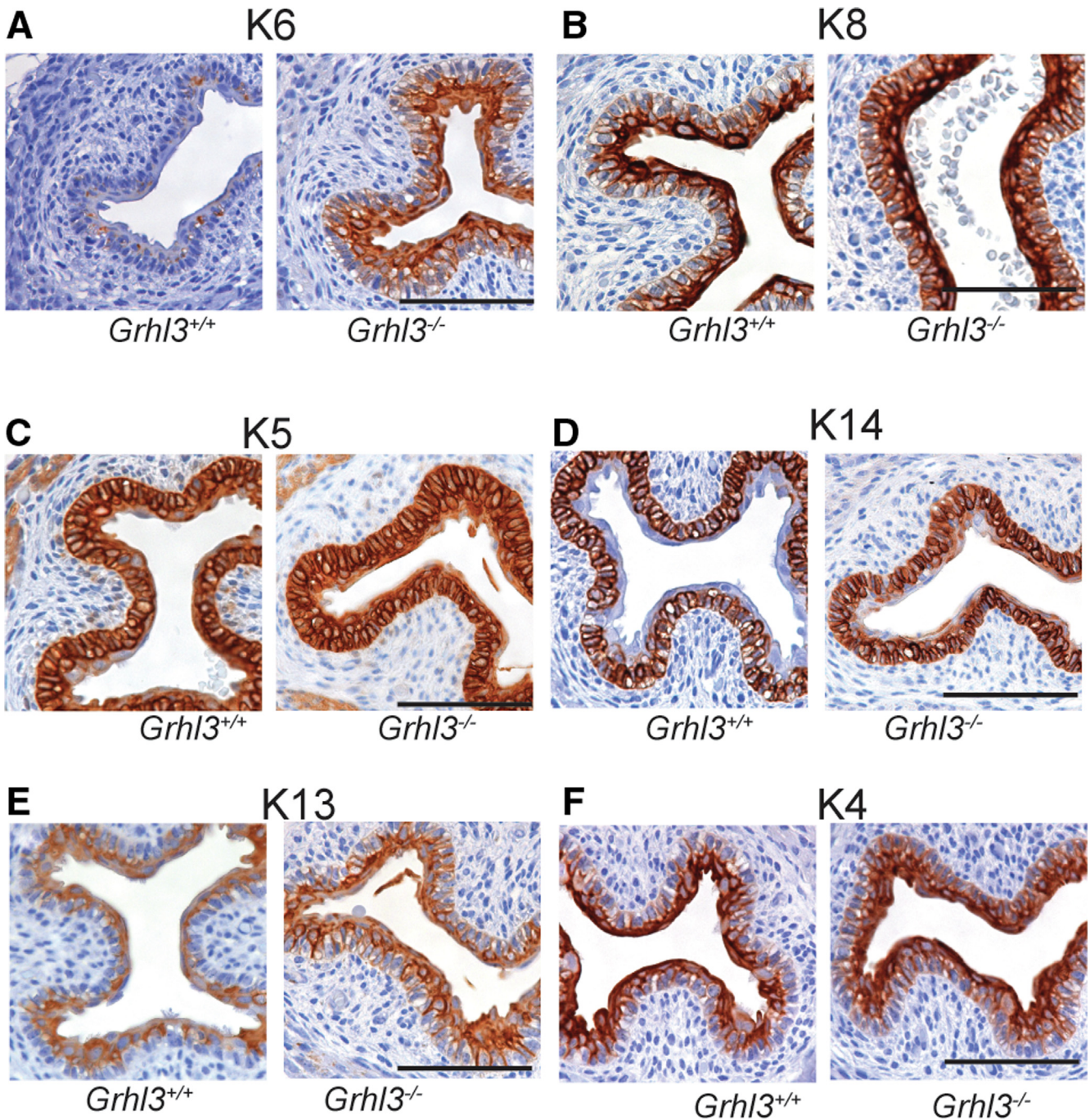


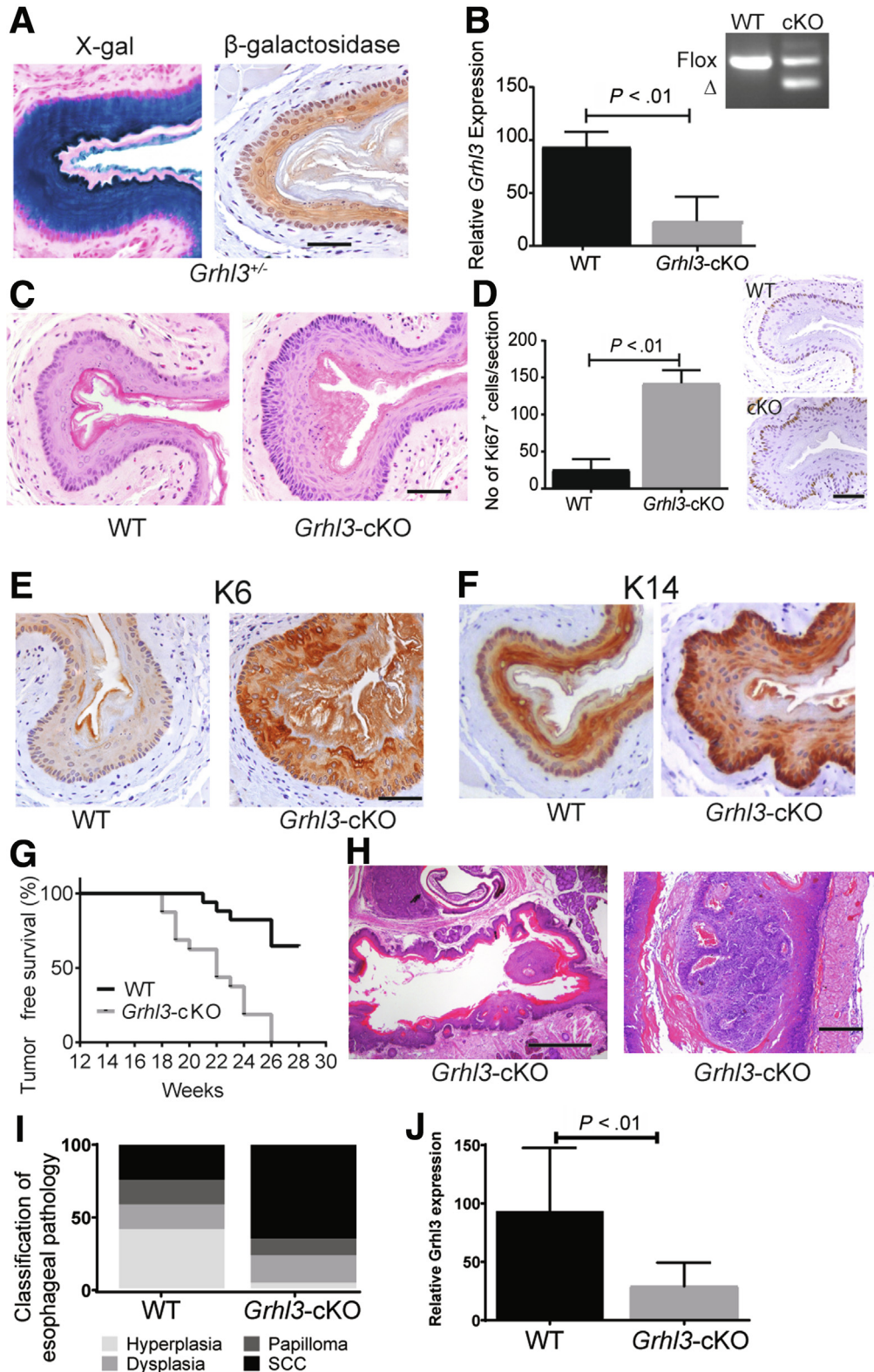
Figure 2. *Grhl3* deletion during embryogenesis causes perturbation of proliferation-differentiation equilibrium of esophageal epithelium. Representative immunohistochemical images of E18.5 *Grhl3*^{+/+} and *Grhl3*^{-/-} mice middle esophagus ($n = 3$ each) stained with K6 (A), K8 (B), K5 (C), K14 (D), K13 (E), and K4 (F) antibodies. Scale bar = 50 μm .

previously to maximize the degree of knockdown, because the recombination efficiency induced by *Cre* is not 100%. This was confirmed by analysis of genomic DNA derived from the esophageal epithelium from *Grhl3*^{+/Δ}/*L2-Cre* mice (*Grhl3-cKO*), which revealed a 1:1 ratio of undeleted (flox) to the deleted *Grhl3* allele (Δ) at 3 months of age (Figure 3B, inset), which remained unchanged up to 12 months (not shown). Despite this, we observed a greater than 70% reduction in *Grhl3* levels in the *Grhl3-cKO* esophageal

epithelium (Figure 3B). With ageing, the *Grhl3-cKO* mice developed a hyperplastic esophageal epithelium, with multiple layers of nucleated cells in the spinous and granular layers (Figure 3C, qualitative observation). Similar to the *Grhl3*^{-/-} embryos, the esophageal epithelium of the *Grhl3-cKO* mice displayed increased numbers of Ki67 positive cells (Figure 3D) and showed enhanced expression of K6 (Figure 3E). K14 expression was also perturbed, occurring at high levels in the basal layer of the *Grhl3-cKO* esophageal

epithelium but not the WT control (Figure 3F). No substantial differences were observed in the expression patterns of K5, K4, and K13 between the WT and *Grhl3*-cKO mice (not shown).

Because of the disruption in the proliferation/differentiation balance observed in the esophageal epithelium of the *Grhl3*-cKO mice, we postulated that loss of *Grhl3* may be a forerunner of esophageal carcinoma. Therefore, we



exposed cohorts of *Grhl3-cKO* mice ($n = 10$) and WT controls ($n = 10$) to the chemical carcinogen 4-nitroquinolene-1 oxide (4-NQO), which has been reported previously to induce esophageal cancer.¹⁴ Mice ingested 4-NQO in drinking water for 16 weeks and were then followed for an additional 12 weeks where 4-NQO was removed from the water. At 26 weeks, 100% of the *Grhl3-cKO* mice exhibited substantial weight loss that necessitated euthanasia, compared with only 40% of WT controls (Figure 3G). Large occluding SCCs were observed in 65% of the *Grhl3-cKO* mice (Figure 3H), whereas 20% of the WT mice had smaller non-occluding SCCs, and none of the WT mice had large occluding SCCs. Histologic scoring of all lesions revealed a marked skewing toward SCC, papillomas, and dysplasia in the *Grhl3-cKO* mice, whereas WT mice displayed predominantly hyperplasia of the esophageal epithelium (Figure 3I). The levels of *Grhl3* expressed in tumors generated in *Grhl3-cKO* mice showed 70% reduction compared with the WT tumors, mirroring the reduction in the premalignant esophageal epithelium (Figure 3J).

Loss of GRHL3 Induces Transcriptome Changes in Esophageal SCCs

To identify the pathways contributing to esophageal SCCs with *Grhl3* deletion, we performed transcriptome analysis in tumors derived from WT and *Grhl3-cKO* mice ($n = 4$). We identified 136 differentially expressed genes in the *Grhl3-cKO* compared with WT tumors (Figure 4A and B), 61 of which showed enhanced expression and 75 that were down-regulated (Table 1). Gene ontology analysis revealed links with expected biological and pathologic processes including epidermis development, skin barrier formation, cell migration, keratinocyte differentiation, apoptosis, and regulation of cell shape but also unanticipated changes in Wnt/ β -catenin signaling (Figure 4C). To confirm the validity of our transcriptome-wide data, we performed quantitative real-time polymerase chain reaction (Q-RT-PCR) on a selection of differentially expressed genes implicated in

carcinogenesis in esophageal SCCs derived from WT and *Grhl3-cKO* mice (Figure 5A). A strong correlation was observed between these data and the transcriptome data in almost all instances, with genes including *Slc1a1*, *Lgr6*, and *Dlg2* all displaying marked up-regulation in the tumors from *Grhl3-cKO* mice, and *Hopx*, *Coch*, and *Aldh1a7* being significantly down-regulated in these cancers. To determine which of these changes in expression could be attributed to loss of *Grhl3*, as opposed to effects induced by the 4-NQO exposure, we examined gene expression in the esophageal epithelium from WT and *Grhl3-cKO* mice that were not treated with the chemical carcinogen (Figure 5B). Surprisingly, many of the marked changes we had observed in the tumors were lost, or even reversed, in the untreated epithelium. For example, expression of *Lgr6* and *Dlg2* was down-regulated in the *Grhl3-cKO* epithelium, and *Coch* was up-regulated. Therefore, we focused our attention on genes that displayed concordant results in the 2 tissues, a prerequisite of driver mutations for cancer that could function cooperatively with additional mutations induced by the carcinogen.

Hopx Is a Direct Target of GRHL3

As a transcription factor, *Grhl3* exerts its biological influence through the regulation of specific target genes. We have previously defined the core GRHL3 consensus DNA binding site (AACCGGTT), which is evolutionarily conserved from *Drosophila* to humans over 700 million years.⁵ Using this sequence, we developed an algorithm to identify direct GRHL3 target genes that was based on (1) the presence of a predicted GRHL3 binding site within 2 kb of the transcription start site; (2) evolutionary conservation of this site across vertebrates; (3) the presence of a chromatin immunoprecipitation (ChIP)-sequencing peak on published datasets; and (4) differential expression in WT versus *Grhl3-cKO* tissues (Figure 5C). This strategy has been highly successful, leading to the identification of critical GRHL3 target genes in wound repair,¹⁵ skin barrier formation,⁵ and epithelial cancers.^{7,8} Because our previous studies have shown that GRHL3

Figure 3. (See previous page). *Grhl3* deletion is a driver of esophageal squamous cell carcinoma. (A) Transverse sections of middle esophagus of *Grhl3* heterozygous mice (*Grhl3*^{+/-}) showing β -galactosidase expression driving from LacZ reporter gene using X-gal staining and antibodies against β -galactosidase. Scale bar = 50 μ m. (B) The mRNA expression of *Grhl3* was detected by quantitative real-time PCR from esophageal epithelium collected from WT ($n = 3$) and *Grhl3-cKO* mice ($n = 6$). Relative gene expression was calculated using HPRT as the housekeeping gene. Data were represented as mean \pm standard deviation of replicates. Statistics were calculated using unpaired, two-tailed Student *t* test. (Inset) Genomic DNA from the esophageal epithelium of 12-week-old WT and *Grhl3-cKO* mice were analyzed using PCR to detect deletion of floxed *Grhl3* allele. The undelleted (flox) band of 425 base pairs and the deleted (Δ) band of 282 base pairs are indicated. (C) Representative H&E images showing moderate hyperplasia of esophageal mucosa in *Grhl3-cKO* mice compared with WT mice. Scale bar = 50 μ m. (D) Graph shows number of Ki67 positive cells in the esophagus in WT ($n = 5$) and *Grhl3-cKO* mice ($n = 3$), enumerated from micrographs immunohistochemically analyzed with Ki67 antibody (representative image shown). Statistics were calculated using unpaired, two-tailed Student *t* test. (E) Representative immunohistochemical images of WT and *Grhl3-cKO* mice esophagus ($n = 3$ each) stained with K6 antibody. Scale bar = 50 μ m. (F) Representative immunohistochemical images of WT and *Grhl3-cKO* mice esophagus ($n = 3$ each) stained with K14 antibody. Scale bar = 50 μ m. (G) Kaplan-Meier survival curve of esophageal tumor-free survival in WT ($n = 10$) and *Grhl3-cKO* mice ($n = 10$). Mice were euthanized upon losing 20% of their body weight. *P* value from the log-rank (Mantel-Cox) test is .04. (H) Representative H&E images of invasive SCC of the esophagus and occluding squamous papilloma in mid esophageal area of *Grhl3-cKO* mice. Scale bar = 50 μ m. (I) Graph representing classification of esophageal lesions in WT ($n = 10$) and *Grhl3-cKO* mice ($n = 10$). (J) The mRNA expression of *Grhl3* was detected by quantitative real-time PCR from esophageal tumors collected from WT ($n = 10$) and *Grhl3-cKO* mice ($n = 8$). Relative gene expression was calculated using HPRT as the housekeeping gene. Data were represented as mean \pm standard deviation of replicates. Statistics were calculated using unpaired, two-tailed Student *t* test (***P* < .01).

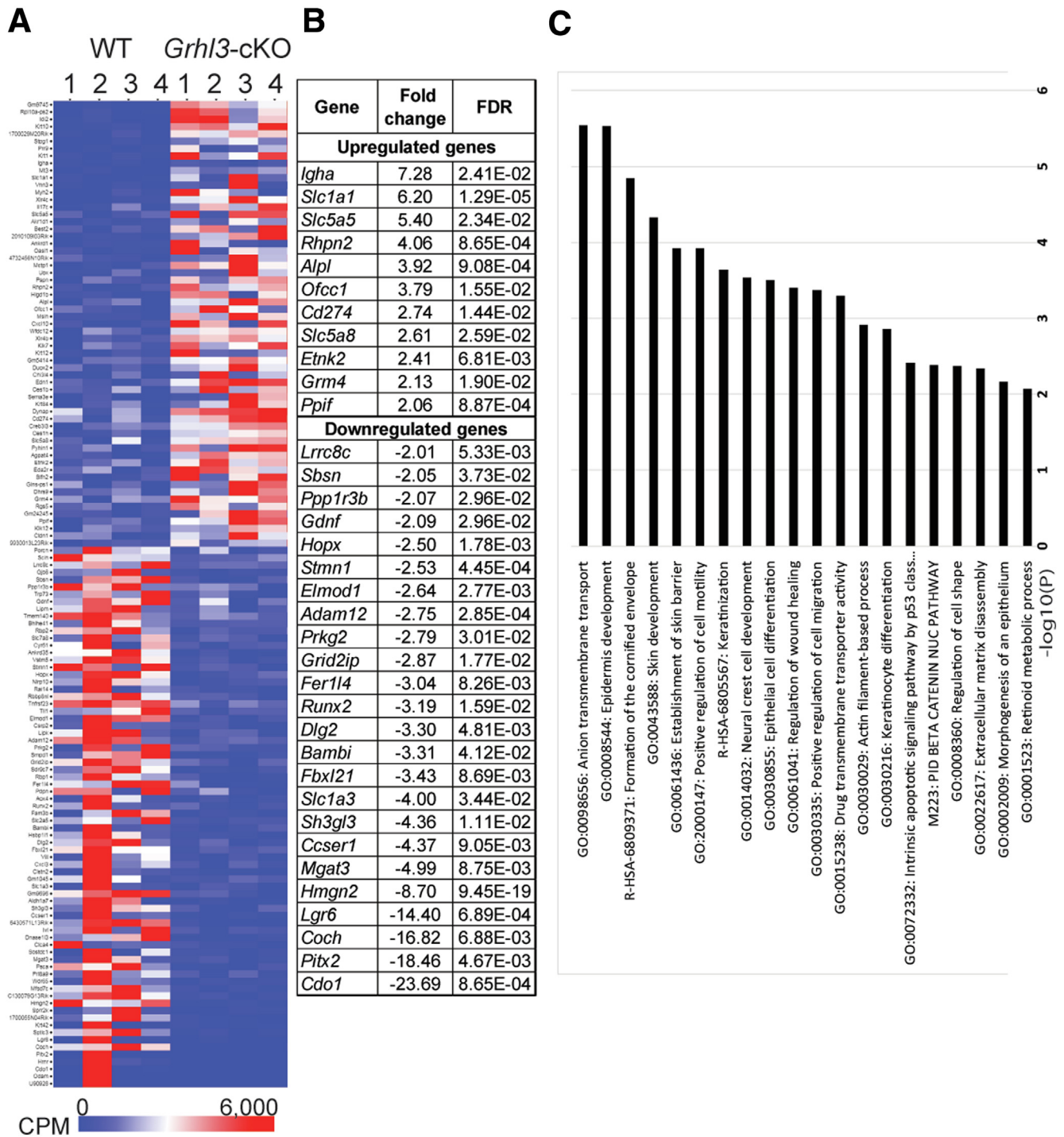


Figure 4. Loss of GRHL3 induces transcriptome changes in esophageal SCC. (A) Heat map of RNA-seq transcriptome analysis showing differential gene expression in ESCC from WT and *Grhl3*-cKO mice. Sixty-one genes were up-regulated, and 75 genes were down-regulated (false discovery rate [FDR] < 0.05) in *Grhl3*-cKO ESCC compared with its WT counterparts. (B) List of genes that are differentially expressed more than 2-fold in *Grhl3*-cKO mice compared with WT mice. (C) Graph shows enriched ontology clusters in differentially expressed genes in *Grhl3*-cKO mice using Metascape analysis.

functions as a tumor suppressor in SCCs from multiple tissue types by transcriptional activation of key target genes, we focused on genes that displayed reduced expression in the absence of *Grhl3* and met all other criteria. On this basis, only *Hopx* fulfilled the stated requirements: (1) a GRHL3 binding

site was identified (Figure 6A); (2) the site was conserved (Figure 6B); and (3) ChIP-seq data identified a clear ChIP-seq peak at the 5' end of the coding exon (Figure 6C and D). We validated the GRHL3 occupancy to the *Hopx* gene at the conserved site by ChIP-Q-PCR (Figure 6E).

Table 1. Differentially Expressed Genes in Grhl3 cKO Esophageal Tumors Compared With WT Tumors

No.	Gene	Expression in cKO tumor vs WT tumor	Fold-change	False discovery rate	<i>P</i> value
1	Gm9745	4.86	28.95	6.19E-14	1.72E-17
2	Rpl10a-ps2	4.52	22.89	1.36E-10	9.49E-14
3	Idi2	4.39	20.91	1.18E-11	5.74E-15
4	Krt10	4.07	16.77	6.19E-14	1.43E-17
5	1700029M20Rik	3.85	14.47	6.54E-07	7.74E-10
6	Stpg1	3.60	12.17	5.91E-06	9.46E-09
7	Prr9	3.39	10.50	5.85E-05	1.35E-07
8	Krt1	3.12	8.72	6.66E-12	2.78E-15
9	Igha	2.86	7.28	0.02408037	.0002295
10	Mt3	2.82	7.06	4.55E-07	5.06E-10
11	Slc1a1	2.65	6.26	1.29E-05	2.16E-08
12	Vnn3	2.59	6.03	0.0212799	.00019541
13	Myh2	2.53	5.77	0.01216068	8.46E-05
14	Xlr4c	2.52	5.75	1.64E-06	2.28E-09
15	Il17c	2.51	5.70	0.0077887	4.77E-05
16	Slc5a5	2.43	5.40	0.02343524	.00021846
17	Akr1d1	2.39	5.25	1.58E-05	2.86E-08
18	Best2	2.29	4.89	0.00957711	6.33E-05
19	2010109I03Rik	2.27	4.84	5.70E-11	3.57E-14
20	Ankrd1	2.26	4.79	0.02390158	.00022447
21	Oasl1	2.24	4.71	5.85E-05	1.36E-07
22	4732456N10Rik	2.14	4.41	0.0017232	7.07E-06
23	Mctp1	2.13	4.37	1.65E-05	3.21E-08
24	Uox	2.12	4.35	0.03069151	.00033521
25	Pspn	2.12	4.34	0.00666409	3.85E-05
26	Rhpn2	2.02	4.06	0.00086482	2.96E-06
27	Higd1b	2.00	4.00	0.0201145	.00018051
28	Alpl	1.97	3.92	0.00090791	3.41E-06
29	Ofcc1	1.92	3.79	0.01549823	.00012183
30	Msln	1.91	3.76	0.00021943	5.50E-07
31	Cxcl10	1.89	3.70	0.00382155	1.91E-05
32	Wfdc12	1.89	3.70	0.00666409	3.83E-05
33	Xlr4b	1.88	3.68	0.00088665	3.19E-06
34	Klk7	1.88	3.68	0.00040908	1.17E-06
35	Krt12	1.85	3.61	0.00192656	8.83E-06
36	Gm5414	1.79	3.45	0.01008913	6.74E-05
37	Duox2	1.78	3.44	0.02711639	.00028295
38	Chi3l4	1.76	3.39	0.02585033	.00025716
39	Edn1	1.73	3.31	2.18E-07	2.22E-10
40	Ces1b	1.65	3.13	0.02522116	.00024914
41	Sema3e	1.59	3.00	0.01982114	.00017512
42	Krt84	1.49	2.82	0.01212562	8.35E-05
43	Dynap	1.48	2.80	0.00206661	9.63E-06
44	Cd274	1.45	2.73	0.0143833	.00010662
45	Creb3l3	1.40	2.65	0.01987858	.00017701
46	Ces1h	1.40	2.64	4.96E-05	1.07E-07
47	Slc5a8	1.38	2.61	0.02594167	.00025987
48	Pyhin1	1.37	2.59	9.02E-05	2.20E-07
49	Agpat4	1.36	2.57	1.80E-05	3.64E-08
50	Etnk2	1.27	2.41	0.0068103	4.03E-05

Table 1. Continued

No.	Gene	Expression in cKO tumor vs WT tumor	Fold-change	False discovery rate	<i>P</i> value
51	Eda2r	1.23	2.34	0.00120149	4.68E-06
52	Sfn2	1.21	2.31	0.00379206	1.87E-05
53	Glns-ps1	1.17	2.25	0.0431795	.00053468
54	Dhrs9	1.10	2.15	0.01280229	9.17E-05
55	Grm4	1.09	2.13	0.01895824	.00016617
56	Rgs5	1.07	2.10	0.00089158	3.29E-06
57	Gm24245	1.06	2.09	0.01721095	.00014367
58	Ppif	1.04	2.06	0.00088665	3.21E-06
59	Klk12	1.00	2.01	0.02484335	.0002385
60	Cldn1	1.00	2.01	0.01531555	.00011933
61	9930013L23Rik	1.00	2.00	0.01159924	7.91E-05
62	Porcn	-1.00	2.00	0.03518776	.00040389
63	Scin	-1.01	2.02	0.00481262	2.64E-05
64	Lrrc8c	-1.02	2.03	0.00532646	3.00E-05
65	Gjb6	-1.04	2.05	0.04022195	.00047847
66	Sbsn	-1.04	2.05	0.03733291	.00043697
67	Ppp1r3b	-1.05	2.07	0.02964876	.00031969
68	Trp73	-1.06	2.09	0.0017369	7.25E-06
69	Gdnf	-1.06	2.09	0.02964876	.00031742
70	Lipm	-1.10	2.14	0.03374927	.00037723
71	Tmem140	-1.11	2.15	0.00280495	1.37E-05
72	Bhlhe41	-1.13	2.19	0.01880423	.00016221
73	Rbp2	-1.18	2.26	0.00481262	2.56E-05
74	Slc7a8	-1.18	2.27	0.0017232	7.00E-06
75	Cyr61	-1.23	2.34	0.02497147	.00024146
76	Ankrd35	-1.30	2.46	0.00057789	1.81E-06
77	Vstm5	-1.33	2.51	0.00183842	8.06E-06
78	Stmn1	-1.34	2.53	0.0004453	1.33E-06
79	Hopx	-1.34	2.53	0.00177526	7.53E-06
80	Nlrp10	-1.34	2.54	5.85E-05	1.38E-07
81	Rai14	-1.37	2.58	0.01740342	.00014649
82	Rbbp8nl	-1.39	2.63	0.00683881	4.09E-05
83	Tnfrsf23	-1.40	2.64	8.51E-08	7.70E-11
84	Tll1	-1.40	2.65	0.02074218	.00018902
85	Elmod1	-1.40	2.65	0.0027709	1.32E-05
86	Csrp2	-1.42	2.68	0.02711639	.00027879
87	Lipk	-1.43	2.69	0.0143833	.00010714
88	Adam12	-1.46	2.75	0.00028507	7.73E-07
89	Prkg2	-1.48	2.79	0.03014967	.00032719
90	Smpd1	-1.52	2.86	8.89E-07	1.11E-09
91	Grid2ip	-1.52	2.87	0.01771554	.00015158
92	Sdr9c7	-1.56	2.94	0.0005923	1.92E-06
93	Rbp1	-1.57	2.98	2.18E-07	2.27E-10
94	Fer1l4	-1.61	3.04	0.008261	5.11E-05
95	Pdpm	-1.62	3.06	0.01455309	.00011136
96	Aox4	-1.62	3.08	0.04713894	.00060338
97	Runx2	-1.68	3.19	0.01589786	.00012784
98	Fam3b	-1.68	3.20	0.01711759	.0001417
99	Slc2a5	-1.69	3.24	0.00040908	1.17E-06
100	Bambi	-1.73	3.31	0.04121757	.00049891

Table 1. Continued

No.	Gene	Expression in cKO tumor vs WT tumor	Fold-change	False discovery rate	P value
101	Hsbn111	-1.74	3.33	0.02522116	.00024596
102	Dlg2	-1.75	3.36	0.00481262	2.62E-05
103	Fbxl21	-1.78	3.43	0.008685	5.49E-05
104	Vill	-1.87	3.66	0.00489226	2.72E-05
105	Cxcl3	-1.88	3.67	0.00025812	6.64E-07
106	Clstn2	-1.89	3.71	0.01589786	.00012829
107	Gm1045	-1.94	3.83	0.0143833	.00010697
108	Slc1a3	-2.01	4.03	0.03439203	.00039237
109	Gm9696	-2.07	4.19	0.0005923	1.94E-06
110	Aldh1a7	-2.10	4.28	0.0004453	1.32E-06
111	Sh3gl3	-2.12	4.36	0.01108265	7.48E-05
112	Ccser1	-2.13	4.37	0.00905438	5.92E-05
113	6430571L13Rik	-2.20	4.58	0.00026295	6.95E-07
114	Ivl	-2.20	4.59	4.42E-05	9.23E-08
115	Dnase1l3	-2.20	4.59	3.74E-09	2.87E-12
116	Clca4	-2.20	4.60	0.00481262	2.59E-05
117	Sostdc1	-2.25	4.75	0.0068103	4.02E-05
118	Mgat3	-2.32	4.99	0.00874882	5.66E-05
119	Psca	-2.43	5.39	9.27E-13	3.22E-16
120	Prl8a9	-2.56	5.88	0.01589786	.00012786
121	Wdr65	-2.70	6.49	0.0013019	5.16E-06
122	Mfsd7c	-2.74	6.67	2.69E-06	3.93E-09
123	C130079G13Rik	-3.02	8.11	7.76E-09	6.48E-12
124	Hmgn2	-3.13	8.73	9.45E-19	6.57E-23
125	Spr2k	-3.14	8.83	1.58E-05	2.75E-08
126	1700055N04Rik	-3.34	10.12	4.99E-06	7.63E-09
127	Krt42	-3.46	10.98	0.0166903	.00013701
128	Sptlc3	-3.66	12.60	8.67E-15	1.21E-18
129	Lgr6	-3.85	14.43	0.000689	2.30E-06
130	Coch	-4.07	16.82	0.00688372	4.17E-05
131	Pitx2	-4.21	18.46	0.00467098	2.40E-05
132	Hmr	-4.28	19.40	1.12E-06	1.48E-09
133	Cdo1	-4.57	23.69	0.00086482	3.01E-06
134	Odam	-5.94	61.26	0.008685	5.50E-05
135	U90926	-7.50	180.90	1.65E-05	3.13E-08
136	Xist	-9.55	750.27	1.49E-11	8.27E-15

NOTE. Data are from RNA-seq analysis.

To determine the localization and expression pattern of *Hopx* in esophageal epithelium, we performed IHC. In WT embryos, the *Hopx* expression correlates with *Grhl3* expression in the suprabasal cell layer and a complete absence of expression in the *Grhl3*^{-/-} embryonic esophageal epithelium (Figure 7A). Similarly, there is reduced *Hopx* expression in the adult esophageal epithelium (Figure 7B). The expression of *Hopx* was reduced in the esophageal epithelium lacking *Grhl3* expression (Figure 7C). *Hopx* has been shown to inhibit Wnt signaling in cardiomyoblasts, airway epithelium, and non-small cell lung cancer by repressing the expression of multiple Wnt ligands,^{16,17} and

alterations in Wnt/ β -catenin signaling were observed in our gene ontology analysis (Figure 4C). To examine this directly, we evaluated the expression of Wnt ligands in the esophageal epithelium of the *Grhl3*-null mice (Figure 7D) and *Grhl3*-cKO mice (Figure 7E and F) using Q-RT-PCR. Wnt2 and Wnt9a were both up-regulated in tissue from *Grhl3*-cKO esophageal tumors and *Grhl3*-null embryos, whereas all other Wnts tested were unchanged. The protein expression of Wnt9a in esophageal tumor sample is also markedly increased in *Grhl3*-cKO mice (data not shown). We then validated HOPX occupancy in the CPG island of the Wnt2 and Wnt9a promoters using ChIP-Q-PCR (Figure 7G).

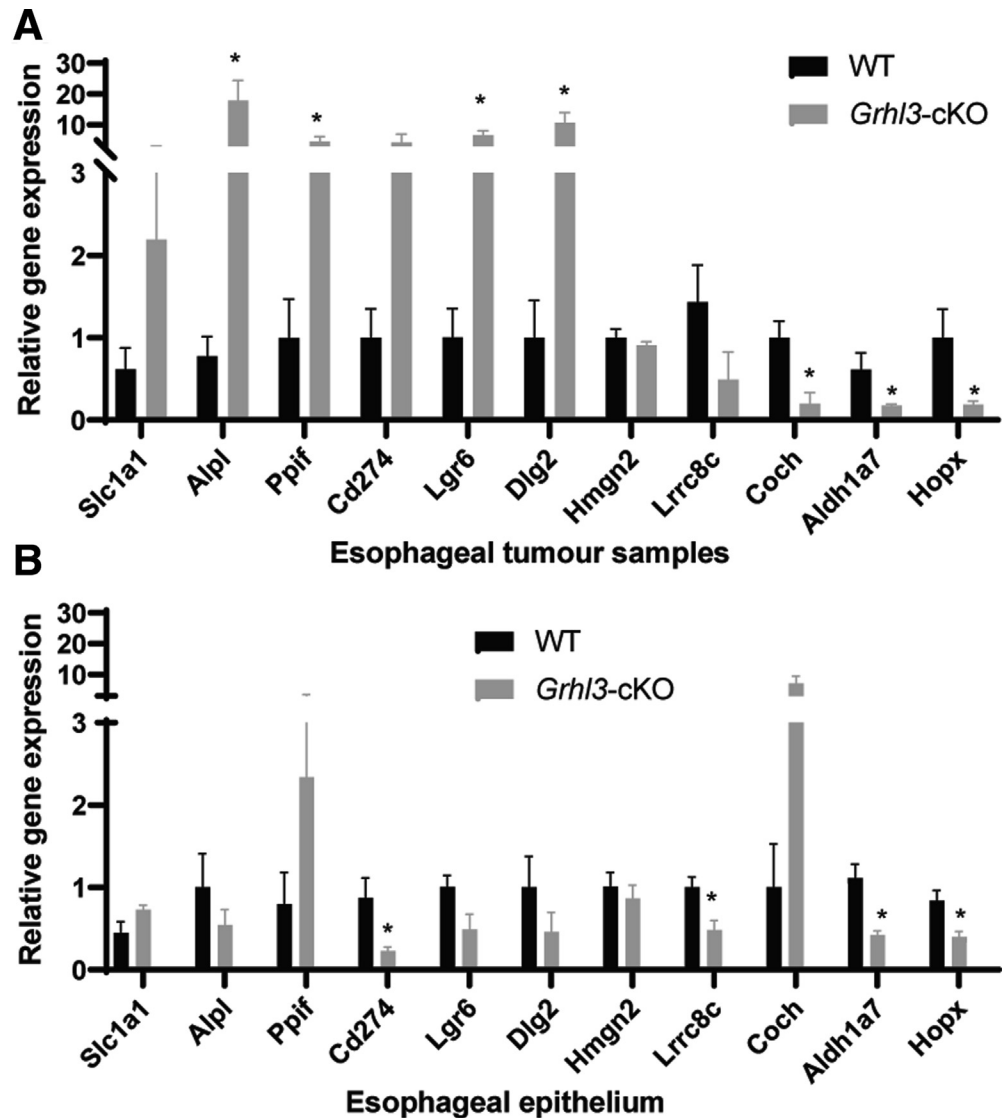


Figure 5. Loss of GRHL3 induces transcriptome changes in esophageal SCC. (A) The mRNA expression of selected genes by Q-RT-PCR from esophageal tumor samples collected from WT and *Grhl3*-cKO mice. Relative gene expression was calculated using HPRT as the housekeeping gene. Data were represented as mean \pm standard deviation of 3–5 replicates. Statistics were calculated using multiple unpaired *t* test using GraphPad prism ($*P < .05$). (C) The mRNA expression of selected genes by Q-RT-PCR from esophageal epithelium collected from WT and *Grhl3*-cKO mice. Relative gene expression was calculated using HPRT as the housekeeping gene. Data were represented as mean \pm standard deviation of 4–8 replicates. Statistics were calculated using multiple unpaired *t* test using GraphPad prism ($*P < .05$). (C) Table showing putative *Grhl3* target genes that are differentially expressed in *Grhl3*-cKO mice.

C

Gene	Fold change in SCC	FDR	Presence of evolutionarily conserved binding site in the proximal promoter	Published Chip-Seq <i>Grhl3</i> bound sites	
				Mice	Human
HOPX	-2.5	1.78E-03	Yes	Yes	Yes
SLC1A1	6.2	1.29E-05	Yes	Yes	Yes
HMG2	-8.7	9.45E-19	Yes	Yes	Yes
SLC5A5	5.4	2.34E-02	No	Yes	Yes
CCSER1	-4.4	9.05E-03	No	Yes	Yes
RBP1	-3.0	2.18E-07	No	Yes	No
ALDH1A7	-4.2	4.45E-04	No	No	No
WDR65	-6.4	1.30E-03	No	No	No
SPR2K	-8.8	1.58E-05	No	No	No
LGR6	-14.4	6.89E-04	No	Yes	Yes
HRNR	-19.9	1.12E-06	No	No	No

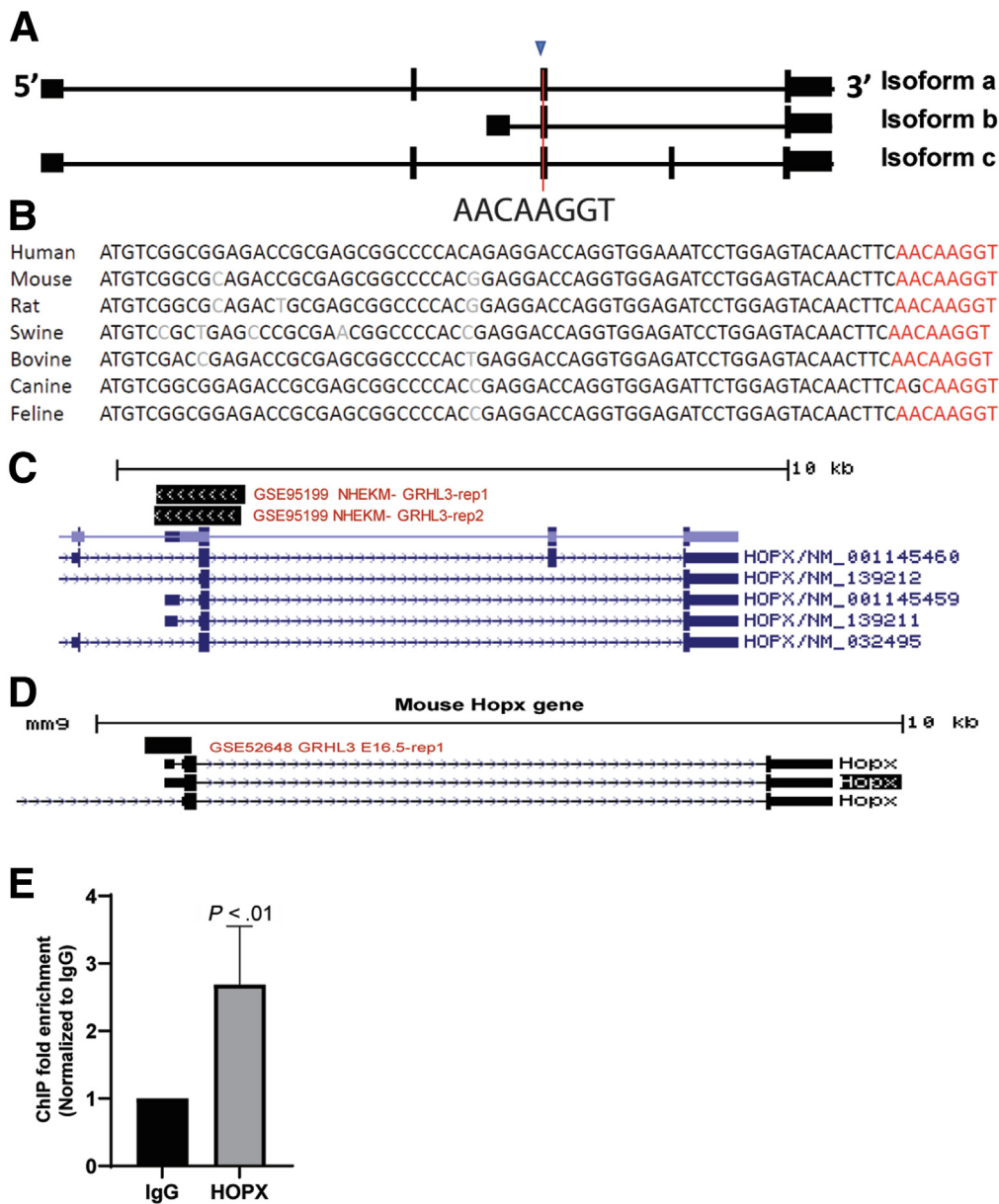


Figure 6. HOPX is a direct target of GRHL3. (A) Location of GRHL3 binding site in the human HOPX genome. Blue arrowhead indicates start codon. (B) Alignment of GRHL3 binding site (red) in the indicated species showing conservation of the site in multiple species. (C) ChIP-seq peak in the promoter region of human HOPX genome from GRHL3 ChIP performed on primary human keratinocytes (NHEK, GSE95199), aligned in the hg19 UCSC genome assembly. (D) ChIP-seq peak in the promoter region of mouse Hopx genome from GRHL3 ChIP performed on E16.5 mouse back skin (GSE52648), aligned in the UCSC mm9 genome assembly. (E) ChIP-Q-PCR from EPC cells demonstrating more than 2-fold enrichment over immunoglobulin G (IgG) in the binding site of HOPX promoter (n = 4 replicates). Statistics were calculated using unpaired, one-tailed Student t test.

β -catenin immunohistochemical analysis of esophageal SCCs revealed a marked increase in expression in *Grhl3-cKO* compared with WT tumors (Figure 8A), suggesting Wnt- β catenin signaling is active specifically in these cancers, in support of our RNA-seq pathway enrichment analysis. We examined several known Wnt pathway target genes altered in other cancers in esophageal tumor samples.^{18,19} Among them, *Met* and *Fgf18* were significantly up-regulated in the ESCCs derived from *Grhl3-cKO* mice compared with WT controls (Figure 8B).

GRHL3 and HOPX Expression Is Reduced in Patient-Derived Esophageal SCC Samples

The genome-wide gene expression in the tumors from 51 ESCC cases to their matched normal tissue samples were studied using Affymetrix microarray.²⁰ The mRNA

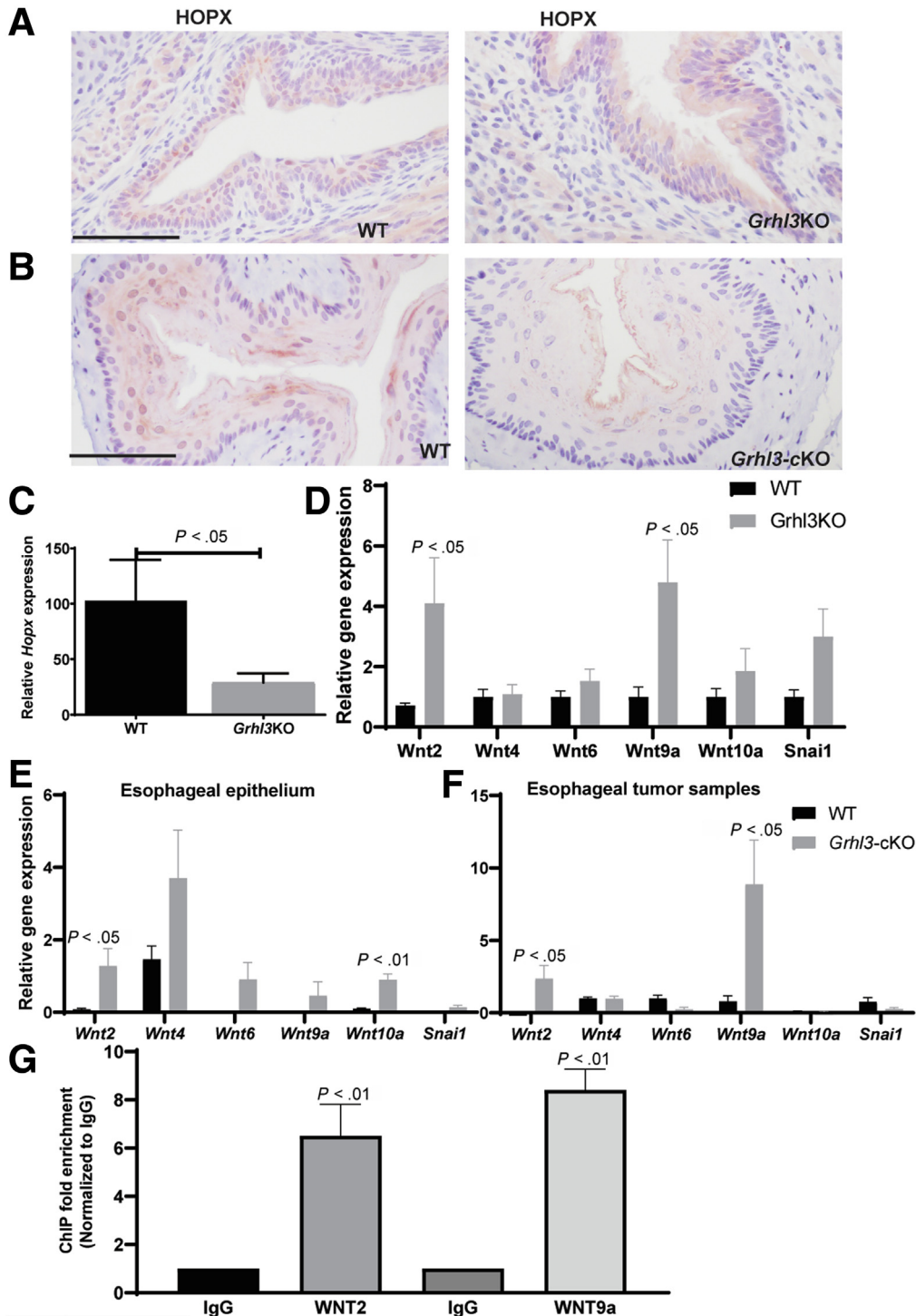
expression of GRHL3 was 2.9-fold down-regulated in ESCC samples compared with normal matched controls (Figure 9A, GSE23400).^{20,21} The expression of HOPX mRNA was also significantly down-regulated in ESCC patient samples (Figure 9B), and the correlation between GRHL3 and HOPX mRNA levels (*r* value 0.88) suggested that they were inter-related (Figure 9C). Similar to mice SCC, WNT2, WNT9A, and MET were up-regulated in these ESCC samples compared with normal matched controls (Figure 9D). However, fibroblast growth factor 18 was unchanged between normal and tumor samples (data not shown). The increased expression of β -catenin in human patient samples indicates this pathway is active in oral squamous cell carcinoma (Figure 9E). These findings support our hypothesis that loss of GRHL3 leads to down-regulation of HOPX and

subsequent activation of the Wnt/ β -catenin pathway. We had validated the expression of GRHL3, HOPX, and WNT9a in human samples (Figure 9E).

Discussion

Using *Grhl3* deleted mouse models and primary human samples we have identified molecular pathways involved in

the pathogenesis of ESCCs, which offer insights for potential novel therapeutics and biomarkers. *Grhl3* is robustly expressed in the esophageal epithelium of embryo and adult mice, and its reduced expression dysregulates the proliferation/differentiation balance and increases the propensity to ESCCs with exposure to the carcinogen 4-NQO. Because it is predominantly expressed in the suprabasal layers, the



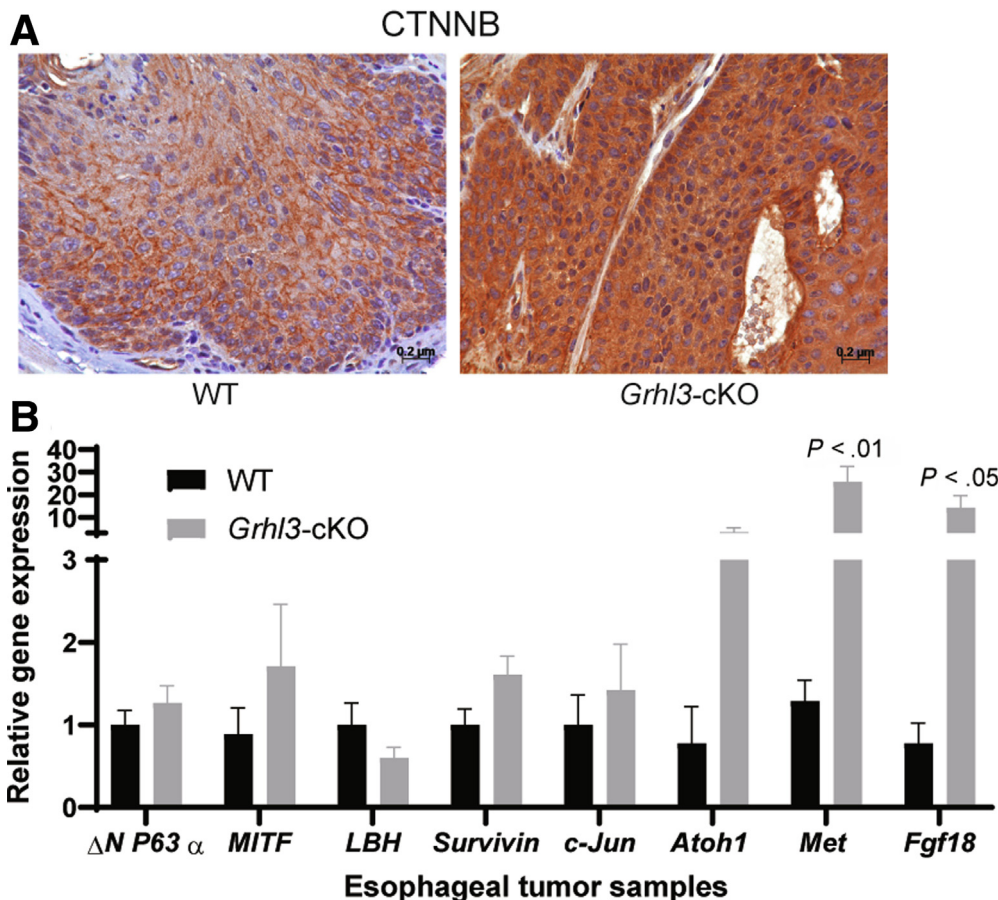


Figure 8. Wnt pathway is dysregulated esophageal SCC samples. (A) Representative immunohistochemical images of WT and *Grhl3*-cKO mice esophageal tumors (n = 3 each) stained with CTNNB antibody. Scale bar = 50 μ m. (B) The mRNA expression of indicated genes by Q-RT-PCR from esophageal tumors collected from WT (n = 8–9) and *Grhl3*-cKO mice (n = 8–9). Relative gene expression was calculated using HPRT as the housekeeping gene. Data were represented as mean \pm standard deviation. Statistics were calculated using multiple unpaired t test using GraphPad Prism.

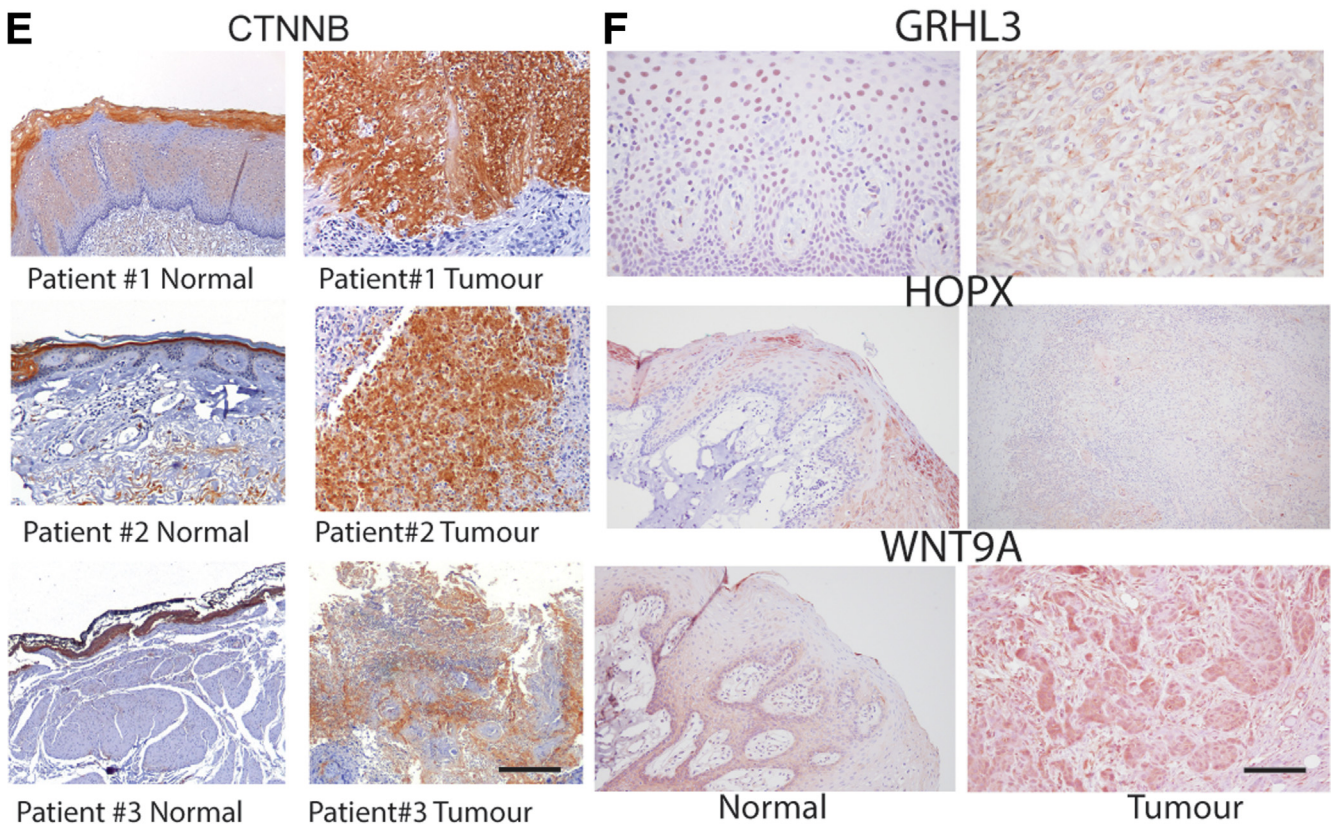
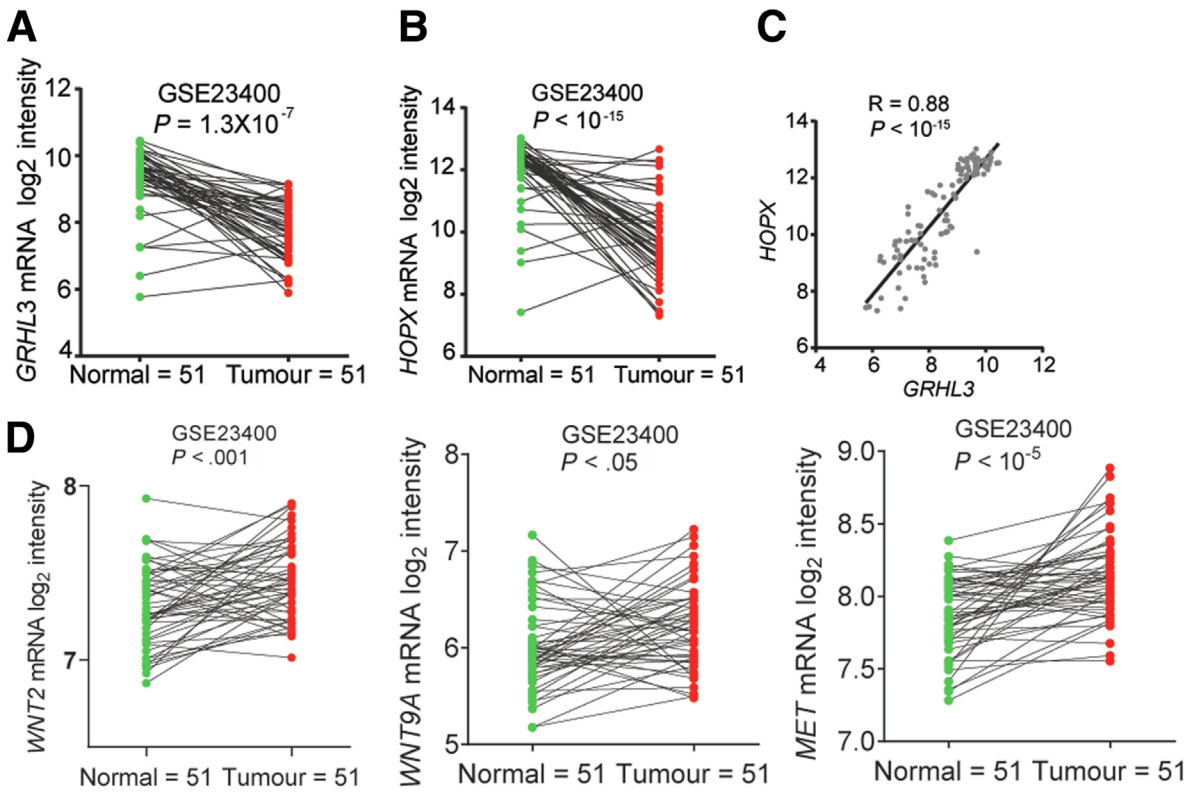
role of GRHL3 in controlling proliferation has been extensively studied in the epidermis. Using single cell RNA-seq, Lin *et al*²² have shown that differentiation of keratinocytes in the epidermis is a gradualistic process, and loss of GRHL3 induces emergence of epidermal stem cells with proliferative potential by suppressing Wnt signaling.

Tissue-specific transcriptional control of GRHL3 in established in skin cancer and head and neck squamous cell carcinoma, and the signaling pathways^{7,8} induced by loss of

Grhl3 in mice differed markedly between the epidermis and oral epithelium. Adding to this complexity of transcriptional control by GRHL3, we identified increased Wnt/ β -catenin signaling in ESCCs, induced by differential regulation of one of the known *Grhl3* target genes, HOPX. HOPX was initially reported as a differentiation marker, and its expression is markedly suppressed in a variety of cancers and is shown to inhibit metastatic progression.^{17,23,24} Even though epigenetic regulation including DNA hypermethylation is

Figure 7. (See previous page.) Reduced expression of HOPX activates Wnt signaling pathway in esophageal epithelium.

(A) Representative immunohistochemical images of middle esophagus from WT E18.5 and *Grhl3*KO embryo esophagus (n = 3 each) stained with HOPX antibody. Scale bar = 50 μ m. (B) Representative immunohistochemical images of middle esophagus from WT and *Grhl3*-cKO adult esophagus (n = 3 each) stained with HOPX antibody. Scale bar = 50 μ m. (C) The mRNA expression of *Hopx* was detected by Q-RT-PCR from esophagus collected from WT (n = 3) and *Grhl3*KO mice (n = 6). Relative gene expression was calculated using HPRT as the housekeeping gene. Data were represented as mean \pm standard deviation. Statistics were calculated using unpaired, two-tailed Student *t* test. (D) The mRNA expression of indicated genes by Q-RT-PCR from esophagus collected from WT (n = 4) and *Grhl3*KO mice (n = 4). Relative gene expression was calculated using HPRT as the housekeeping gene. Data were represented as mean \pm standard deviation. Statistics were calculated using multiple unpaired *t* test using GraphPad prism. (E) The mRNA expression of indicated genes by Q-RT-PCR from esophageal epithelium collected from WT (n = 6) and *Grhl3*-cKO mice (n = 6). Relative gene expression was calculated using HPRT as the housekeeping gene. Data were represented as mean \pm standard deviation. Statistics were calculated using multiple unpaired *t* test using GraphPad Prism. (F) The mRNA expression of indicated genes by Q-RT-PCR from esophageal tumors collected from WT (n = 5–6) and *Grhl3*-cKO mice (n = 5–6). Relative gene expression was calculated using HPRT as the housekeeping gene. Data were represented as mean \pm standard deviation. Statistics were calculated using multiple unpaired *t* test using GraphPad Prism. (G) ChIP-Q-PCR from EPC cells demonstrating more than 4-fold enrichment over immunoglobulin G (IgG) in WNT2 and WNT9a promoter (n = 3 replicates). Statistics were calculated using unpaired, one-tailed Student *t* test.



reported as a mechanism of reduced expression of HOPX in nasopharyngeal carcinoma,²³ it does not play a role in HOPX expression in lung adenocarcinoma and human epidermal keratinocytes.^{17,25} This holds true in the case of ESCCs, where its expression is transcriptionally regulated by GRHL3.

Our integrated approach using patient-derived ESCC samples and mouse models identified the Wnt/ β -catenin pathway as the downstream signaling target of GRHL3 and HOPX. One of the up-regulated Wnt ligands, Wnt2, in both mice and human ESCCs is significantly associated with poor clinical outcomes in patients and has been shown to activate canonical Wnt/ β -catenin signaling pathway in esophageal cancer cells.²⁶ Wnt2 has been shown to be secreted by tumor fibroblasts, and it is probable that reduced expression of HOPX removes the transcriptional control leading to enhanced expression of these secretory ligands. Through whole-genome analysis, it has been shown that HOPX regulates multiple Wnt genes, and in tissues, with HOPX deletion there is an expansion of Wnt signaling.¹⁶ We propose that the tumor suppressor function of HOPX observed in multiple cancers is due to its ability to repress Wnt signaling, which is based on the evidence from ESCC. The presence of stem cells in the esophagus is still under debate; however, using organoids, it has been shown that a non-quiescent stem cell population resides in the basal epithelium of mice esophagus, and Wnt has been shown to regulate esophageal self-renewal.²⁷ It is possible that these stem cells are activated with reduced expression of GRHL3 and HOPX through Wnt signaling leading to ESCC.

Our work identified a molecular signature in ESCCs that provides a clear rationale for using targeted therapies in this cancer. Several Wnt antibodies (vantictumab, inhibitor of frizzled receptor) and β -catenin inhibitors (PRI-724) are already phase 1 clinical trials in solid cancers²⁸ and are promising agents for ESCC. There are challenges in inhibiting the Wnt pathway, because this pathway plays an important role in the maintenance of stem cells and regeneration of tissues and organs. Specific inhibitors targeting cancer stem cells are required to overcome side effects; nevertheless, ESCC is a potential solid cancer that could benefit from Wnt/ β -catenin inhibition in select patients with low GRHL3 expression levels.

Methods

Experimental Animals

All experiments were preapproved by the AMREP Animal Ethics Committee. The generation and genotyping of

Grhl3^{+/-} have been described previously.¹¹ To generate Grhl3-cKO mice, transgenic B6. Cg-Tg(ED-L2-cre) 267Jkat/Nci¹³ were purchased from NCI Mouse Repository and crossed with Grhl3^{+/-} mice. The resultant L2Cre⁺/Grhl3^{+/-} mice were crossed with Grhl3^{fl/fl} mice to provide the Grhl3 ^{Δ /-}/L2Cre⁺ experimental animals (Grhl3-cKO). Both male and female mice were used in the experiments presented here.

Esophageal tumors were induced in 5-month-old Grhl3-cKO mice through the administration of 50 μ g/mL 4-NQO (Sigma-Aldrich) in drinking water for 16 weeks, followed by reversion to regular water and monitoring for 24 weeks.⁸ All animals underwent weekly oral cavity examination and were euthanized by cervical dislocation when exhibiting significant weight loss or at week 24. A complete autopsy was performed on all animals, and histopathologic lesions in the esophagus were scored by a certified pathologist.

Immunohistochemistry

For IHC, tissues were collected and fixed in 4% paraformaldehyde overnight and analyzed as described previously.⁷ Antibodies used for IHC and the dilutions used are shown in Table 2.

RNA Preparation and Quantitative Real-Time Polymerase Chain Reaction

For gene expression analysis, esophagus from E18.5 Grhl3^{+/+} and Grhl3^{-/-} embryos and esophageal epithelium from WT and Grhl3-cKO mice were homogenized in Trizol (Invitrogen), and RNA was extracted according to the manufacturer's instructions. Esophageal tumors were macro-dissected from the slides after staining with Histogene staining solution (Thermo Fisher Scientific). RNA was extracted using RNeasy Micro Kit (Qiagen) according to the manufacturer's instructions. Quantitative real-time PCR was carried out as described previously,¹¹ with hypoxanthine-guanine phosphoribosyltransferase serving as the internal control in all experiments. A Student *t* test was used to determine statistical differences in expression levels, with *P* values <.05 considered significant, and the results were analyzed using GraphPad Prism. The error bars in all expression analyses represent the standard deviation. The primers used for Q-RT-PCR are shown in Table 3.

Figure 9. (See previous page). **GRHL3 and HOPX expression is reduced in patient-derived esophageal SCC samples leading to activation of Wnt signaling pathway.** (A) GRHL3 mRNA expression in 51 oral squamous cell carcinoma (OSCC) samples compared with its own paired normal tissue, calculated from GSE23400. Statistics were calculated using unpaired, two-tailed Student *t* test, and *P* values are indicated on the graph. (B) HOPX mRNA expression in 51 OSCC samples compared with its own paired normal tissue, calculated from GSE23400. Statistics were calculated using unpaired, two-tailed Student *t* test, and *P* values are indicated on the graph. (C) Correlation between GRHL3 and HOPX mRNA expression in patient samples calculated from GSE23400. Pearson *r* method using GraphPad prism is used to calculate the correlation between the mRNA expression. (D) WNT2, WNT9A, and MET mRNA expression in 51 OSCC samples compared with its own paired normal tissue, calculated from GSE23400. Statistics were calculated using unpaired, two-tailed Student *t* test, and *P* values are indicated on the graph. (E) Representative immunohistochemical images of 3 human patient esophageal samples immunohistochemically stained with CTNNB. Scale bar = 50 μ m. (F) Representative immunohistochemical images of human patient esophageal samples immunohistochemically stained with GRHL3, HOPX, and WNT9A. Scale bar = 50 μ m.

Table 2. Details of Antibodies Used for Immunohistochemistry and Their Concentration

Antibodies	Catalogue no.	Concentration	Species
β -galactosidase	ab9361	1:1000	Chicken polyclonal
Ki67	ab6667	1:100	Rabbit monoclonal
K6	PRB-169P	1:500	Rabbit polyclonal
K8	MABT329M	1:50	Rat monoclonal
K5	PRB-160P	1:100	Rabbit polyclonal
K14	PRB-155P	1:2000	Rabbit polyclonal
K4	ab9004	1:400	Mouse monoclonal
K13	ab92551	1:1000	Mouse monoclonal
CTNNB	CST9562	1:300	Rabbit polyclonal
HOPX	PA5-114744	1:100	Rabbit polyclonal
WNT9A	PA5-96871	1:100	Rabbit polyclonal
GRHL3	HPA059960	1:100	Rabbit polyclonal

Transmission Electron Microscopy

Ultrathin (~80 nm) sections of the transverse plane of each esophagus were examined with a Hitachi H-7500 transmission electron microscope operated at 80 kv. Digital images were captured with a Gatan multi-scan camera using the software digital micrograph.

RNA-seq Sample Preparation and Sequencing

Qiagen RNeasy micro kits were used to extract RNA from esophageal tumors from WT and *Grhl3-cKO* mice treated with 4-NQO. Specifically, tumors were macro-dissected from frozen cryosections to avoid contamination with normal esophageal tissue. RNA was quantified using Qubit RNA

Table 3. Primer Sequences for Quantitative Real-time Polymerase Chain Reaction

Species	Gene	Sense	Antisense
Mouse	<i>Grhl3</i>	AAGGAAGATGTCGAATGAACTTG	TCGTCCTCATTACTGTAGGGAAA
Mouse	<i>Slc1a1</i>	GGATGCCATGTTGGACCTGA	CCCGCTTGGTTTTGTACTGC
Mouse	<i>Alpl</i>	TCGGAACAACCTGACTGACC	GTCAATCCTGCCTCCTTCCA
Mouse	<i>Ppif</i>	CCGACGAGAACTTCACACTGA	ATGCTTGCCATCTAGCCAGTC
Mouse	<i>Cd274</i>	CGCCTGCAGATAGTTCCCAA	AGCCGTGATAGTAAACGCC
Mouse	<i>Lgr6</i>	CTGTCCGCTGACTGCTCC	ACTGAGGTCTAGGTAAGCCGT
Mouse	<i>Dlg2</i>	TCCTTAGCAGCACATGCCC	TCGATACTTCTTTACGTTAGTCCG
Mouse	<i>Hmgn2</i>	GCGAGGTTGTCTGCTAAACC	GCGAGGTTGTCTGCTAAACC
Mouse	<i>Lrrc8c</i>	CCCCCAGAGATTAATGTGGCT	GAACTCGGTCACCGGAATCA
Mouse	<i>Coch</i>	GAGGGAGCGGTTCCCATTC	ATGCTGGACACTGACGCATA
Mouse	<i>Aldh1a7</i>	TTTGGCTGTCCCTGTCCAAT	ACCATGTTCCGCCAGTTCTC
Mouse	<i>Hopx</i>	GCCCCAGTGTAAAGAAATGGT	GTGACGGATCTGCACTCTGA
Mouse	Δ NP63 α	GAGCAGCCTTGACCAGTCTC	GGTTCGTGACTGTGGCTCA
Mouse	<i>MITF</i>	GCAAGAGGGAGTCATGCAGT	AGAACTGCTGCTCTTCAGAGGT
Mouse	<i>LBH</i>	GATCGGCTGAGATGACCGAG	ATGGGTCCGAAAGATCTGA
Mouse	<i>Survivin</i>	AGAACAAAATTGCAAAGGAGACCA	CTGGGATGCGTGGCTTAGAT
Mouse	<i>c-Jun</i>	GGGAGCATTTGGAGAGTCCC	TTTGCAAAGTTTCGCTCCCG
Mouse	<i>Atoh1</i>	GTGCGATCTCCGAGTGAGAG	GGGATAAGCCCCGAACAACA
Mouse	<i>Met</i>	TCTGGGAGCTCATGACGAGA	CCTCGTACAAGGCGTCTGGA
Mouse	<i>FGF18</i>	TGGGGAAGCCTGATGGTACT	CCCTTGGGGTAACGCTTCAT
Mouse	<i>Wnt2</i>	CTCTCGGTGGAATCTGGCTC	CCTGTAGCTCTCATGTACCACC
Mouse	<i>Wnt4</i>	CAGGAAGGCCATCTTGACACAC	GTCTTTACCTCGCAGGAGCC
Mouse	<i>Wnt6</i>	ACTGGGGGTTTCGAGAATGTC	TCTCTCGGATGTCTGCTGC
Mouse	<i>Wnt9a</i>	GCCTACTTCGGGCTGACG	GGTCGCAGGCCTTGTAGTG
Mouse	<i>Wnt10a</i>	CCGAGAGCCTCACAGAGACA	GTTCTCCATCACCGCCTGC
Mouse	<i>Snai1</i>	AAGATGCACATCCGAAGCCA	ATGGCTTCTACCAGTGTGG

Table 4. Primer Sequences for Chromatin Immunoprecipitation Polymerase Chain Reaction

Species	Gene	Sense	Antisense
Human	HOPX	GCAGAAGCGATGGGAGATCAT	CACAGAGGACCAGGTGGAAA
Human	WNT2	CCGAGAGGGGCGTTCATATT	CTGGCCTTTATCGCTCGCTG
Human	WNT9a	GGAAGTACTTACAGGGGGC	AAGTCCAGAGGGCAAGTGTG

fluorometry (Invitrogen), and RNA integrity was assessed with the Agilent Bioanalyzer 2100 (Agilent Technologies). Illumina's TruSeq stranded mRNA chemistry was used to produce libraries that were poly-A selected to remove structural RNA, which was performed by Micromon (Monash University, Melbourne, Australia). The libraries were sequenced to produce at least 20 million paired-end 75 base pair reads per sample using Illumina NextSeq500 in High-Output mode. The FastQC software (S. Andrews, FastQC: A Quality Control Tool for High Throughput Sequence Data. 2015. Available from: <http://www.bioinformatics.babraham.ac.uk/projects/fastqc>) was used to assess the quality of the raw sequence data, and all samples passed the quality control. Sequences were then mapped to the mouse reference genome (Grcm38, Ensembl) using RNAsik-pipe/1.4.7 (<https://github.com/MonashBioinformaticsPlatform/RNAsik-pipe/tree/1.5.3>), and gene-level counts were obtained by the feature Counts tool.²⁹ Further analysis was carried out using the edgeR³⁰ package configured Degust software (<https://zenodo.org/record/3501067#.YYi4E3jxVhE>). Counts per million were calculated for each gene to standardize for differences in library size, and filtering was carried out to retain genes with a baseline expression level of at least 1.0 CPM in 3 or more samples.

ChIP-Q-PCR

Approximately 50 million EPC cells were cross-linked for 10 minutes in 0.75% formaldehyde at room temperature. After quenching cross-linking for 5 minutes with 125 mmol/L glycine and washing the cells in cold phosphate-buffered saline, the cells were lysed in 50 mmol/L Tris-HCl, pH 8.1, 1% sodium dodecyl sulfate, 10 mmol/L EDTA, and protease inhibitor (added freshly). Chromatin was sheared to 200–500 base pair fragments using the S220 Covaris sonicator (105 peak incident power; duty factor 7; 200 cycles/burst; 40 seconds; USA). The sheared DNA was immunoprecipitated with anti-Grhl3Ab (Sigma HPA059960-100 μ L), HOPX Polyclonal Ab (PA5-114744, Invitrogen), or Rabbit IgG antibody (~10 μ g chromatin, 0.5 μ g antibody for ChIP-Q-PCR) overnight. Protein-A agarose beads were added to each reaction for 1 hour at 4°C the following day. The magnetic beads were then washed in a series of buffers including a low salt buffer (20 mmol/L Tris-HCl, pH 8.1, 150 mmol/L NaCl, 2 mmol/L EDTA, 0.1% sodium dodecyl sulfate, 1% Triton X-100), a high salt buffer for 15 minutes (20 mmol/L Tris-HCl, pH 8.1, 500 mmol/L NaCl, 2 mmol/L EDTA, 0.1% sodium dodecyl sulfate, 1% Triton X-100), a LiCl buffer (10 mmol/L Tris-HCl, pH 8.1, 0.25 mol/L LiCl, 1 mmol/L EDTA, 1% NP-40, 1% deoxycholic acid), and finally

with TE buffer, with each wash lasting for 5 minutes. Complexes were eluted in 1% sodium dodecyl sulfate, 0.1 mol/L NaHCO₃. DNA was uncross-linked, and either Q-PCR was performed for regions of interest (primer sequences in Table 4). For ChIP-Q-PCR experiments, Ct values for immunoprecipitation (either specific antibody or immunoglobulin G) were normalized to input. Fold-change enrichment between specific antibody (Grhl3 or HOPX) and immunoglobulin G is shown for ChIP-Q-PCR data. The data included are representative of ChIPs from at least 3 replicates and are the mean \pm standard deviation.

All authors had access to the study data and had reviewed and approved the final manuscript.

References

1. Bray F, Ferlay J, Soerjomataram I, et al. Global cancer statistics 2018: GLOBOCAN estimates of incidence and mortality worldwide for 36 cancers in 185 countries. *CA Cancer J Clin* 2018;68:394–424.
2. Smyth EC, Lagergren J, Fitzgerald RC, et al. Oesophageal cancer. *Nat Rev Dis Primers* 2017;3:17048.
3. Njei B, McCarty TR, Birk JW. Trends in esophageal cancer survival in United States adults from 1973 to 2009: a SEER database analysis. *J Gastroenterol Hepatol* 2016;31:1141–1146.
4. Alcolea MP, Greulich P, Wabik A, et al. Differentiation imbalance in single oesophageal progenitor cells causes clonal immortalization and field change. *Nat Cell Biol* 2014;16:615–622.
5. Ting SB, Caddy J, Hislop N, et al. A homolog of *Drosophila* grainy head is essential for epidermal integrity in mice. *Science* 2005;308:411–413.
6. Ting SB, Wilanowski T, Cerruti L, et al. The identification and characterization of human Sister-of-Mammalian Grainyhead (SOM) expands the grainyhead-like family of developmental transcription factors. *Biochem J* 2003; 370(Pt 3):953–962.
7. Darido C, Georgy SR, Wilanowski T, et al. Targeting of the tumor suppressor GRHL3 by a miR-21-dependent proto-oncogenic network results in PTEN loss and tumorigenesis. *Cancer Cell* 2011;20:635–648.
8. Georgy SR, Cangkrama M, Srivastava S, et al. Identification of a novel proto-oncogenic network in head and neck squamous cell carcinoma. *J Natl Cancer Inst* 2015; 107:1–13.
9. Yu WY, Slack JM, Tosh D. Conversion of columnar to stratified squamous epithelium in the developing mouse oesophagus. *Dev Biol* 2005;284:157–170.
10. Auden A, Caddy J, Wilanowski T, et al. Spatial and temporal expression of the Grainyhead-like transcription

- factor family during murine development. *Gene Expr Patterns* 2006;6:964–970.
11. Ting SB, Wilanowski T, Auden A, et al. Inositol- and folate-resistant neural tube defects in mice lacking the epithelial-specific factor Grhl-3. *Nat Med* 2003;9:1513–1519.
 12. Yu Z, Lin KK, Bhandari A, et al. The Grainyhead-like epithelial transactivator Get-1/Grhl3 regulates epidermal terminal differentiation and interacts functionally with LMO4. *Dev Biol* 2006;299:122–136.
 13. Nakagawa H, Wang TC, Zukerberg L, et al. The targeting of the cyclin D1 oncogene by an Epstein-Barr virus promoter in transgenic mice causes dysplasia in the tongue, esophagus and forestomach. *Oncogene* 1997;14:1185–1190.
 14. Tang XH, Knudsen B, Bemis D, et al. Oral cavity and esophageal carcinogenesis modeled in carcinogen-treated mice. *Clin Cancer Res* 2004;10(Pt 1):301–313.
 15. Caddy J, Wilanowski T, Darido C, et al. Epidermal wound repair is regulated by the planar cell polarity signaling pathway. *Dev Cell* 2010;19:138–147.
 16. Jain R, Li D, Gupta M, et al. Integration of Bmp and Wnt signaling by Hopx specifies commitment of cardiomyoblasts. *Science* 2015;348:aaa6071.
 17. Cheung WK, Zhao M, Liu Z, et al. Control of alveolar differentiation by the lineage transcription factors GATA6 and HOPX inhibits lung adenocarcinoma metastasis. *Cancer Cell* 2013;23:725–738.
 18. Boon EM, van der Neut R, van de Wetering M, et al. Wnt signaling regulates expression of the receptor tyrosine kinase met in colorectal cancer. *Cancer Res* 2002;62:5126–5128.
 19. Thakur R, Mishra DP. Pharmacological modulation of beta-catenin and its applications in cancer therapy. *J Cell Mol Med* 2013;17:449–456.
 20. Su H, Hu N, Yang HH, et al. Global gene expression profiling and validation in esophageal squamous cell carcinoma and its association with clinical phenotypes. *Clin Cancer Res* 2011;17:2955–2966.
 21. Rhodes DR, Yu J, Shanker K, et al. ONCOMINE: a cancer microarray database and integrated data-mining platform. *Neoplasia* 2004;6:1–6.
 22. Lin Z, Jin S, Chen J, et al. Murine interfollicular epidermal differentiation is gradualistic with GRHL3 controlling progression from stem to transition cell states. *Nat Commun* 2020;11:5434.
 23. Ren X, Yang X, Cheng B, et al. HOPX hypermethylation promotes metastasis via activating SNAIL transcription in nasopharyngeal carcinoma. *Nat Commun* 2017;8:14053.
 24. Yap LF, Lai SL, Patmanathan SN, et al. HOPX functions as a tumour suppressor in head and neck cancer. *Sci Rep* 2016;6:38758.
 25. Yang JM, Sim SM, Kim HY, et al. Expression of the homeobox gene, HOPX, is modulated by cell differentiation in human keratinocytes and is involved in the expression of differentiation markers. *Eur J Cell Biol* 2010;89:537–546.
 26. Fu L, Zhang C, Zhang LY, et al. Wnt2 secreted by tumour fibroblasts promotes tumour progression in oesophageal cancer by activation of the Wnt/beta-catenin signalling pathway. *Gut* 2011;60:1635–1643.
 27. DeWard AD, Cramer J, Lagasse E. Cellular heterogeneity in the mouse esophagus implicates the presence of a nonquiescent epithelial stem cell population. *Cell Rep* 2014;9:701–711.
 28. Krishnamurthy N, Kurzrock R. Targeting the Wnt/beta-catenin pathway in cancer: update on effectors and inhibitors. *Cancer Treat Rev* 2018;62:50–60.
 29. Liao Y, Smyth GK, Shi W. featureCounts: an efficient general purpose program for assigning sequence reads to genomic features. *Bioinformatics* 2014;30:923–930.
 30. Robinson MD, McCarthy DJ, Smyth GK. edgeR: a Bioconductor package for differential expression analysis of digital gene expression data. *Bioinformatics* 2010;26:139–140.

Received December 6, 2021. Accepted November 23, 2022.

Correspondence

Address correspondence to: Smitha Rose Georgy, BVSc, MVSc, PhD, DACVP, Veterinary Anatomic Pathology, Faculty of Veterinary and Agricultural Sciences, The University of Melbourne, 250 Princess Highway, Werribee, Victoria 3030, Australia. e-mail: s.georgy@unimelb.edu.au.

Acknowledgments

The authors thank Monash bioinformatics platform, animal facility and histopathology platform for the assistance in the experiments. They acknowledge the Victorian biobank for providing human patient samples.

CRedit Authorship Contributions

Smitha Rose Georgy, BVSc, MVSc, PhD, MANZCVS Diplomate ACVP (Conceptualization: Lead; Funding acquisition: Equal; Investigation: Lead; Methodology: Lead)

Diar Riyanti Rudiarmoko (Investigation: Supporting)
Alana Auden (Methodology: Supporting; Validation: Supporting)
Darren Partridge (Investigation: Supporting; Methodology: Supporting; Validation: Supporting)

Tariq Butt (Data curation: Supporting; Investigation: Supporting; Methodology: Supporting)

Seema Srivastava (Data curation: Supporting; Investigation: Supporting; Methodology: Supporting)

Nick Wong (Data curation: Supporting; Software: Supporting)

Marina Rose Carpinelli (Formal analysis: Supporting)

Dijina Swaroop (Methodology: Supporting; Software: Supporting)

Mirjana Bogeski (Data curation: Supporting; Validation: Supporting),
Stephen M. Jane (Conceptualization: Lead; Formal analysis: Equal; Supervision: Lead; Writing – review & editing: Equal)

Conflicts of interest

The authors disclose no conflicts.

Funding

Supported by Cancer Australia's Priority-driven Collaborative Cancer Research Scheme in conjunction with the National Health and Medical Research Council project grant and The Garnett Passé and Rodney Williams Memorial Foundation Research Training Fellowship to SRG.